Reports

Meteorite Impact Ejecta: Dependence of Mass and Energy Lost on Planetary Escape Velocity

Abstract. *The calculated energy efficiency of mass ejection for iron and anorthosite objects striking an anorthosite planet at speeds of 5 to 45 kilometers per second decreases with increasing impact velocity at low escape velocities. At escape velocities of* $>10^5$ *and* $>2 \times 10^4$ *centimeters per second, respectively, the slower impactors produce relatively less ejecta for a given impact energy. The impact velocities at which ejecta losses equal meteorite mass gains are found to be approximately 20, 35, and 45 kilometers per second for anorthosite objects and approximately 25, 35, and 40 kilometers per second for iron objects striking anorthosite surfaces for the gravity fields of the moon, Mercury, and Mars.*

A central problem in many theories of the evolution of the solar system and planetary accretion is determining the amounts of material and energy which escape the planet in a meteorite impact event. We have calculated the mass of ejecta (M_e) and the associated energy (E_e) escaping planets as functions of impact and escape velocities (V_e). Our results are obtained from the computed flow fields (the spatial distribution of particle velocities, the complete axisymmetric stress tensor in cylindrical coordinates, the material density, and the internal energy density) induced by the impact of iron (Fe) and gabbroic anorthosite (An) spheres onto a half-space of An, denoted by Fe→An and An→An, at impact velocities of 5 to 45 km/sec (*1*). A numerical method utilizing the mass, momentum, and energy conservation relations in finite-difference approximation, within an Eulerian (fixed in space) computational grid, was used to determine the impact-induced flows (*2*). An equation of state was constructed which accounts for the polymorphism and thermodynamic properties of silicates and iron over a wide range of temperatures and pressures and a material response model was constructed having the appropriate rheological and dynamic yielding properties. The compressive strength properties of lunar sample 15418, a recrystallized gabbroic anorthosite breccia, were taken to be representative of the model planetary surface. This rock has a dynamic strength under uniaxial strain of ~35 kbar (*3*) and an assumed tensile strength of 0.5 kbar (*1*). These parameters are critical for calculating the partitioning between internal and kinetic energy in the ejecta.

A previous study (*1*) of the partitioning upon impact of meteorite energy into internal and kinetic energy residing in projectile and planetary target material has demonstrated that for Fe and An impacts, the percentage of projectile kinetic energy transformed into internal energy ranges from 70 at 5 km/sec to 85 at 30 km/sec for an An→An impact, and from 74 to 91, at the same speeds, for an Fe→An impact (*1*). At low velocities (for both cases) much of the internal energy (approximately 50 percent at 5 km/sec) is produced by the plastic work resulting from the high compressive yield strength of the rock. The remainder of the internal energy results from shock heating. The relative percentage of the impact energy residing in the kinetic energy of the planetary surface ranges from 10 to 7 for the An→An impacts and 9 to 7 for the Fe→An impacts over the range 5 to 30 km/sec. Most of this energy resides in the ejecta; that is, the elastic energy (seismic efficiency) of the impact process is low (~0.01 to 0.1 percent) (*4*).

The amount of mass escaped (M_e) as a function of V_e for the An→An and Fe→An impacts relative to the incident meteorite kinetic energy (E_{KE}) and meteorite mass (M_m) is shown in Figs. 1 and 2. Figure 1 implies that the efficiency with respect to incident energy of ejecting mass at velocities exceeding a given value of V_e decreases with increasing impact velocity in the range of escape velocities $<10^5$ cm/sec for An→An impacts and $<2 \times 10^4$ cm/sec for the Fe→An im-

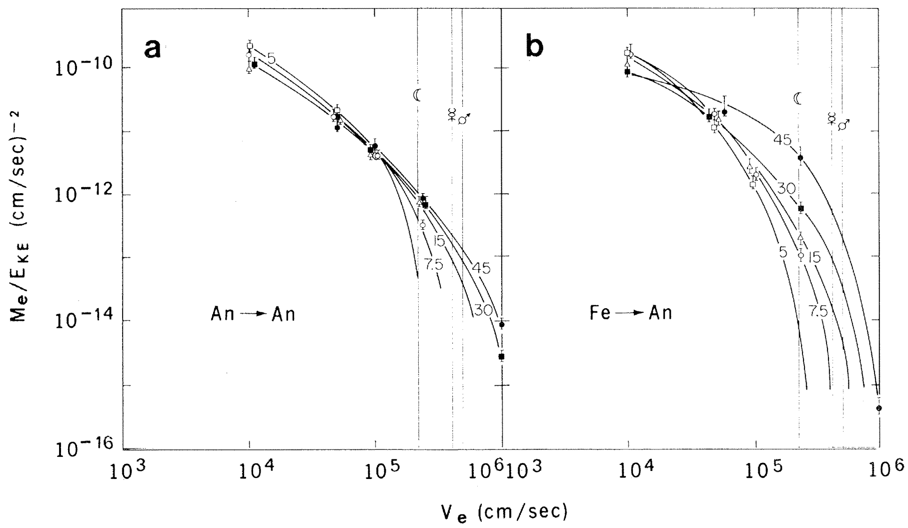

Fig. 1. Ratio of mass of ejecta, M_e, to initial kinetic energy of meteorite, E_{KE}, plotted against escape velocity, V_e. The numbers on the curves indicate impact velocities in kilometers per second. The uncertainties indicated are computational in origin. Escape velocities for the moon, Mercury, and Mars are indicated by light vertical lines. (a) Anorthosite impacting anorthosite. (b) Iron impacting anorthosite.

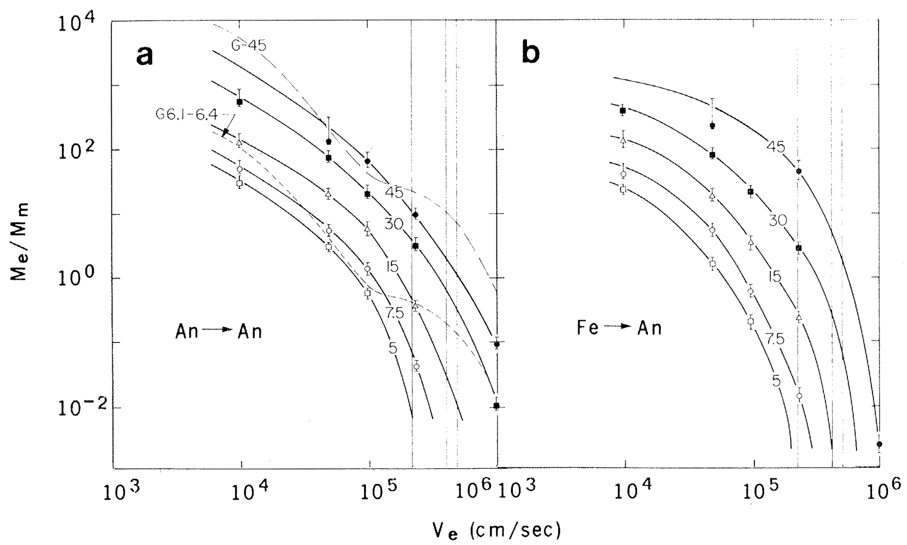

Fig. 2. Ratio of mass ejected, M_e, to meteorite mass, M_m, plotted against escape velocity, V_e. (a) Anorthosite impacting anorthosite. The curves labeled *G 6.1—6.4* and *G-45* are from experiments of Gault *et al.* (*6*), in which 2-mm-diameter aluminum spheres impacted basalt in the indicated velocity range. The curve for a 45 km/sec impact was inferred (*6*). (b) Iron impacting anorthosite.

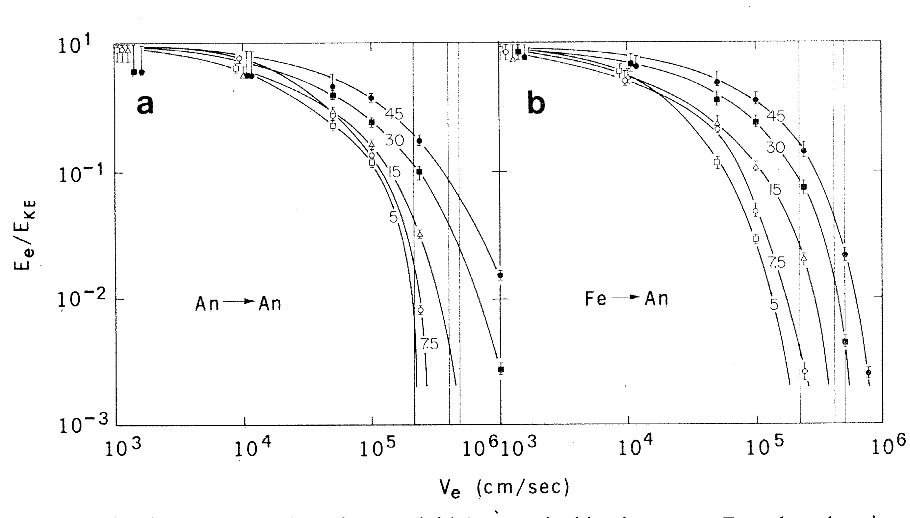

Fig. 3. Ratio of total energy ejected, E_e, to initial meteorite kinetic energy, E_{KE}, plotted against escape velocity, V_e. (a) Anorthosite impacting anorthosite. (b) Iron impacting anorthosite.

pacts. In the range of escape velocities exceeding those given above, this trend is reversed.

The ratios M_e/M_m, for different impact velocities, for the An→An and Fe→An impacts (Fig. 2, a and b) indicate that for impact velocities of 30 km/sec and less, the less dense An meteorite is more efficient in creating high-speed ejecta. This is because it does not penetrate as deeply as the Fe meteorite and hence deposits its energy closer to the surface. However, in the range of V_e between $\sim 2 \times 10^4$ and 5×10^5 cm/sec, a 45 km/sec iron meteorite ejects relatively more mass than an An meteorite. The mass ejection energy efficiency of an iron meteorite increases at an impact velocity of 45 km/sec (and probably at higher speeds) because the expansion of the vaporized planetary surface material initially constricts the transient cavity. Later, when the growth of the cavity has diminished, the partially trapped meteorite vapor expands and excavates the overlying planetary surface material (Fig. 1b). This effect has previously been demonstrated (*1*). The relative mass (M_e/M_m) lost for the An→An impact at lunar escape velocity, 2.4 km/sec, varies from less than 0.01 at 5 km/sec to 12.0 at 45 km/sec. For the Fe→An impacts, M_e/M_m varies from less than 0.01 at 5 km/sec to 50.0 at 45 km/sec. An important consideration is the critical value of impact velocity at which the mass lost balances the mass gained. In the cases of the moon, Mercury, and Mars these critical velocities are $\simeq 20$, 35, and 45 km/sec for an An→An impact and $\simeq 25$, 35, and 40 km/sec for an Fe→An impact, respectively.

On the basis of the peak in mean square velocity of objects currently striking the moon, 15 to 18 km/sec (*5*), we calculate that the amount of material presently escaping the moon is less than would be predicted from the photographic experiments of Gault *et al.* (*6, 7*). Considering the differences in projectile and target materials, our calculations and the estimates based on the experiments (*6*) are in approximate agreement for V_e between 10^4 and 10^5 cm/sec; however, at $V_e \gtrsim 10^5$ cm/sec the experimental results imply an order of magnitude greater mass loss. The critical impact velocity for the moon obtained by Gault *et al.* (*6*) is $\simeq 10$ km/sec, as compared to $\simeq 20$ km/sec for our An→An impact calculations. These differences may result from the high assumed target strength; the basalt is probably considerably weaker than An. The production of experimental craters less than 1 m in diameter (*8*) suggests that strength effects are important on this scale. Schneider (*9*) impacted steel projectiles on a strong Duran glass target at 4.4 km/sec and determined that the mass in the ejecta with V_e exceeding 3 km/sec was only 7.5×10^{-5} M_m, which is more consistent with our calculations.

The relative amount of meteorite kinetic energy lost (E_e/E_{KE}) ranges from approximately 90 percent at $V_e \sim 10^3$ cm/sec to ≤ 1 percent at $V_e \sim 10^6$ cm/sec (Fig. 3, a and b). At the lunar escape velocity, the amount of energy lost from the moon for An→An impacts ranges from 0.8 percent at an impact velocity of 7.5 km/sec to 17 percent at 45 km/sec, and similarly for Fe→An impacts, E_e/E_{KE} ranges from 0.3 percent at 7.5 km/sec to 15 percent at 45 km/sec. These results illustrate a more general conclusion: a less dense meteorite will lose relatively more of its energy on impact with a planetary surface for fixed values of impact velocity and V_e. An extrapolation of our results implies that cometary objects would not transfer their energy to a planet as effectively as iron or stony objects. In addition, if the strength of the planetary surface is less than that of the modeled consolidated rock, we expect that more energy and mass will be lost at $V_e < 10^4$ cm/sec, whereas not much change in the fraction of energy and mass lost at $V_e > 10^5$ cm/sec is expected. This is because the energy that is consumed by plastic work in strong rocks would be available for conversion into kinetic energy in weak rocks, and thus would increase the amount of ejecta at low velocities from weak rocks and unconsolidated regoliths.

JOHN D. O'KEEFE
THOMAS J. AHRENS
Division of Geological and Planetary Sciences, California Institute of Technology, Pasadena 91125

References and Notes

1. J. D. O'Keefe and T. J. Ahrens, in *Proceedings of the 6th Lunar Science Conference*, R. B. Merrill, Ed. (Pergamon, New York, 1975), p. 2831; in *Proceedings of the 7th Lunar Science Conference*, R. B. Merrill, Ed. (Pergamon, New York, 1976), p. 3007; T. J. Ahrens and J. D. O'Keefe, in *Impact and Explosive Cratering*, D. J. Roddy, R. O. Pepin, R. B. Merrill, Eds. (Pergamon, New York, in press); J. D. O'Keefe and T. J. Ahrens, *Phys. Earth Planet. Inter.*, in press.
2. L. J. Hageman and J. M. Walsh, *Systems, Science and Software Report 3SR-350* (Systems, Science and Software, La Jolla, Calif., 1977), vol. 1.
3. T. J. Ahrens, J. D. O'Keefe, R. V. Gibbons, in *Proceedings of the 4th Lunar Science Conference*, W. A. Ghose, Ed. (Pergamon, New York, 1973), p. 2575.
4. P. H. Schultz and D. E. Gault, in *Proceedings of the 6th Lunar Science Conference*, R. B. Merrill, Ed. (Pergamon, New York, 1975), p. 2845.
5. H. A. Zook, in *ibid.*, p. 1653.
6. D. E. Gault, E. M. Shoemaker, H. J. Moore, *NASA Spec. Publ. TND-1767* (1963).
7. Whereas the experiments of Gault *et al.* (6) were carried out on solid basalt, similar high-speed photographic recordings of impacts in sand [D. Breslau, *J. Geophys. Res.* **75**, 3987 (1970)] surprisingly indicated almost equivalent energy partitioning of projectile energy into the ejecta.
8. H. J. Moore, R. W. MacCormack, D. E. Gault, paper presented at the 6th Symposium on Hypervelocity Impact, Cleveland, Ohio, April–May 1963.
9. E. Schneider, *Moon* **13**, 173 (1975).
10. J.D.O. is also with TRW Inc., Redondo Beach, Calif. 92078. This research was supported by NASA grant NSG 7129. We appreciate critical comments on the manuscript by H. Melosh and R. Jeanloz and the computational assistance of M. Lainhart. This is contribution No. 2928 of the Division of Geological and Planetary Sciences, California Institute of Technology.

24 June 1977; revised 22 August 1977

Evidence for a Pollination-Drop Mechanism in Paleozoic Pteridosperms

Abstract. *A noncellular substance containing pollen and spores has been discovered protruding from the micropyle of a seed fern ovule of Middle Pennsylvanian age. This provides direct evidence that pollination-drop mechanisms comparable to those of many extant gymnosperms characterize some Paleozoic pteridosperms.*

The pteridosperms are an early group of fossil seed plants with fernlike leaves and leafborne reproductive organs. The taxon extends from Late Devonian through Jurassic time, with some of the best-known permineralized specimens preserved in sediments of Pennsylvanian age. The mechanism of pollination in these and other Paleozoic seed plants is widely regarded as similar to that of many extant gymnosperms, where a sticky exudate protrudes from the micropyle of the ovule (*1*, *2*). Pollen adheres to or becomes immersed in the droplet, and is either drawn toward the pollen chamber as the droplet shrinks (due to desiccation) or floats upward toward the tip of the nucellus (*2*).

Previous reports of pollination-drop mechanisms in fossil plants have been based primarily on the occurrence of similar structural features in extant and fossil ovules, rather than on the physical presence of a preserved droplet. Moreover, conflicting interpretations of the function performed by the pollen-receiving structures of some fossil ovules (*3*) leave these aspects of the reproductive

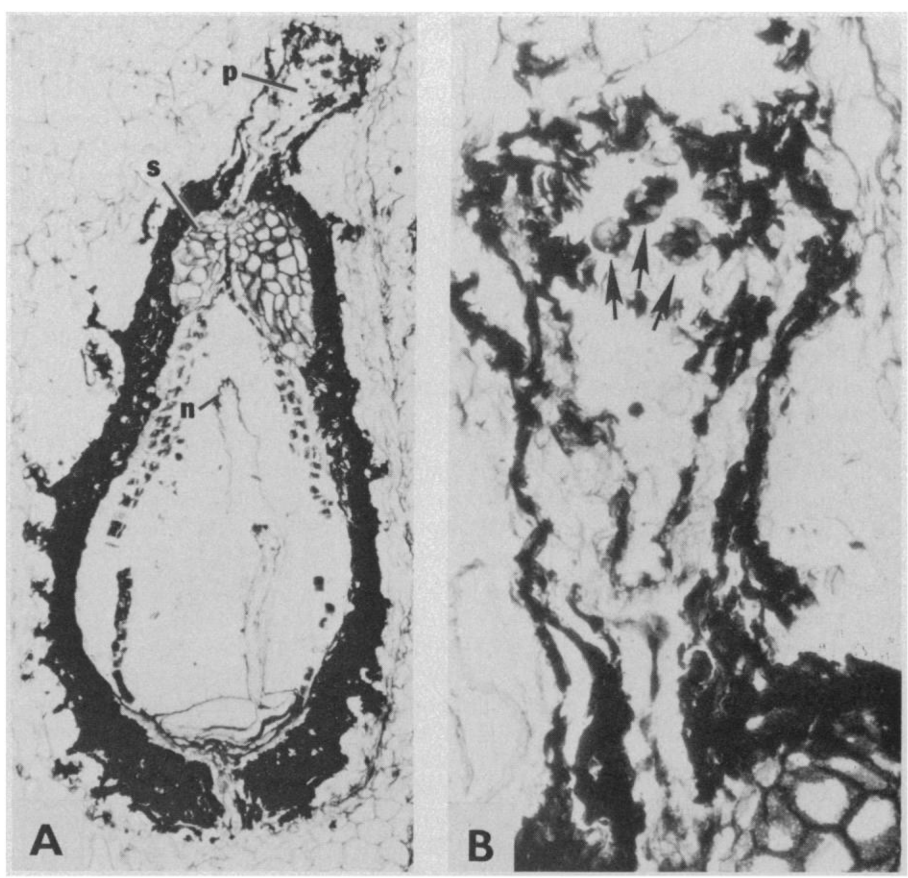

Fig. 1. *Callospermarion*-type ovule with pollination droplet protruding from the micropyle. (A) Midlongitudinal section of immature ovule (*n*, nucellus; *p*, pollination droplet; and *s*, sclerotesta) (× 42). (B) Pollination droplet at the micropylar end of the ovule. The arrows indicate the positions of three palynomorphs (× 155).